Focused on New Trends in Fatigue and Fracture

Mixed mode fracture: numerical evaluation and experimental validation using PMMA specimens

Sérgio A.G. Pereira, Sérgio M.O. Tavares, Paulo M.S.T. de Castro

Faculdade de Engenharia da Universidade do Porto - FEUP, Rua Dr. Roberto Frias, 4200-465 Porto, Portugal
ptcastro@fe.up.pt

ABSTRACT. The analysis of mixed mode crack propagation has been more accessible with the development of new numerical tools, allowing to evaluate the influence of non-mode I loadings in the crack path and in the growth rate. The aim of this work is to analyse the propagation of pre-existing cracks under pure mode I, pure mode II and unstable mixed mode I-II loading conditions. Numerical simulations with two-dimensional models created in Abaqus software were performed, and the results obtained were compared with the analytical and experimental results. To determine *T*-stress and stress intensity factors, the conventional finite element method was used, post-processed with the modified virtual crack closure technique (mVCCT) and / or the J-integral. The extended finite element method (XFEM) is also used to predict the crack trajectory under different loading conditions.

The experimental procedures were performed in three- and four-point bending tests on single edge notch specimens of PMMA, in which a natural pre-crack was created by small impacts on a blade located over the pre-existing machined notch. The four-point bending test was performed with an asymmetrical configuration. Varying the locations of supports and loading points with respect to the crack plane, this configuration allows to create pure mode II and mixed-mode I-II situations. The three-point bending test was performed in the conventional manner, with only the distance from the load line to the crack plane being varied.

KEYWORDS. LEFM, Mixed mode I-II, Stress intensity factor, Extended finite element method, Crack path.

INTRODUCTION

Mixed mode fracture is a subject addressed by several theoretical approaches. A diversity of specimens has been proposed for testing, while several numerical techniques for modelling crack propagation under mixed-mode loading are in use. For mode II fracture toughness testing, for ex., a variety of approaches are still under

consideration, see *e.g.* [1]. In mixed-mode fracture the fit of theoretical models and experimental data displays some variation, as exemplified by PMMA results of Erdogan and Sih [2] or Smith, Ayatollahi, Pavier [3]. Given the continued interest in the topic of mixed mode fracture, the present work discusses mixed mode fracture modelling and testing, illustrating the levels of approximation attained using several techniques, with PMMA as an experimental case study.

Fracture mechanics under mixed mode loading in planar structures has been less explored than the pure mode I, due to the difficulty of the crack behavior characterization in mode II and III. Several testing methods, based on different geometries and loading conditions, are available in the literature. For instance, in planar geometries, the Compact Tension Shear (CTS) [4] and the Brazilian disk [5] are common geometries for mixed mode fracture testing, allowing to evaluate the material behavior for different degrees of mixity. However, other simple geometries can be used for these studies, as is the case of the Single Edge Notch specimen (SEN).

Considering conventional axial testing machines, two types of tests are possible for planar geometries: *(i)* axial tension/compression tests and *(ii)* bending tests. Bending tests are advantageous for testing in mixed mode since crack growth with any combination of mode I/mode II can be performed by changing the position of the crack in relation to the load locations.

In this work, SEN specimens were tested in bending for the characterization of toughness of Poly(methyl methacrylate) (PMMA) under mixed mode conditions, and advanced numerical formulations were used to simulate non-pure mode I loading conditions. Possible influence of *T*-stress in the results was assessed and results were compared with those obtained using flat plates with inclined cracks tested by Erdogan and Sih, [2]. For planar specimens, crack path predictions are based on 2D Finite Element (FE) analysis and consideration of K_I and K_{II} in the frame of suitable K_{eq} criteria; numerical tools, such as the modified virtual crack closure technique (mVCCT), [6], and the extended finite element method (XFEM), [7], are used. The experimental results are compared with the results obtain by Erdogan and Sih, [2], and Rebelo, [8], among others.

The 4-point asymmetric bending test allows to study the behaviour of a specimen subjected pure mode II or mixed mode I-II, see *e.g.* [9,10]. Considering an asymmetric load, it is possible to measure the fracture toughness in pure mode II (K_{IIc}) and to vary the ratio K_I / K_{II} or K_{II} / K_I by changing the distance of application of the load to the plane of the crack (S_0), Fig. 1.
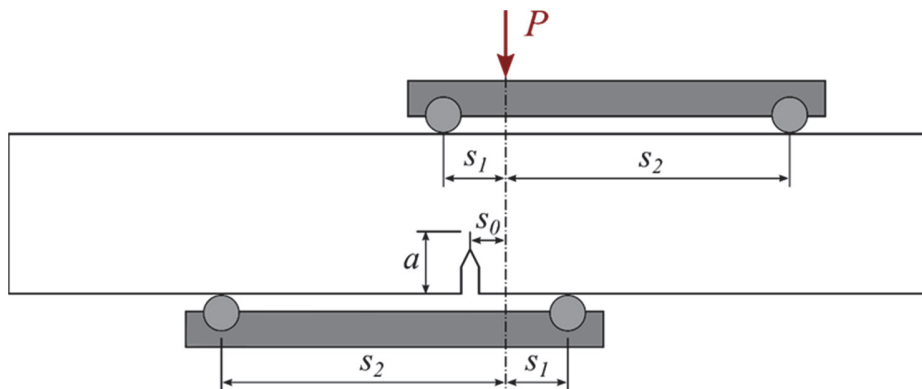

Figure 1: Mixed mode I-II in a 4-point bending test.

For $S_0 = 0$ (force applied in the plane of the crack) the bending moment is null and there is only shear force; representing a situation of pure mode II. For mixed-mode analysis, the variation of S_0 influences the mode I component, resulting in different shear stress and bending moment combinations at the plane of the crack. According to Wang et al., [11], the stress intensity factors for mixed mode are given by:

$$K_I = \frac{\eta Q \sqrt{\pi a}}{W t} Y_I \qquad (1)$$

$$K_{II} = \frac{Q \sqrt{\pi a}}{W t} Y_{II} \qquad (2)$$

The values of the geometric factors Y_I and Y_{II} can be obtained from [11]. Q is the shear force on crack tip and can be obtained by Y_{II}, P being the applied load. W is the specimen width, t is the specimen thickness and a the crack length. The relative length between the point of application of the load and the pre-crack is given by $\eta = S_0 / W$.

The 3-point eccentric bending load test also allows to test mixed mode I-II crack propagation. By varying the position of the crack in relation to the plane of application of the load (in the middle of the specimen), the measurement of the toughness in mode I (K_{Ic}) or the analysis of mixed mode crack propagation are possible, Fig. 2.
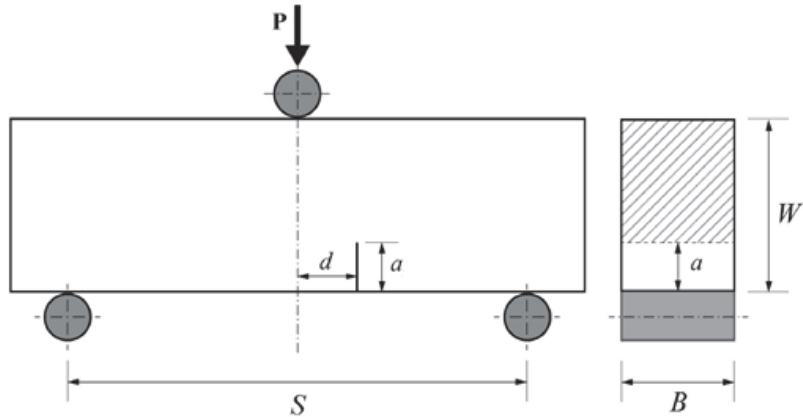

Figure 2: Specimen for the eccentric 3-point bending test, SEN, [12].

Pure mode II loading is not conceivable with this set-up since the bending moments are zero only in the support points. Belli et al., [12], show that mode I and II stress intensity factors can be obtained by the following expressions:

$$K_I = \sigma_0 Y_I \sqrt{\pi a} \tag{3}$$

$$K_{II} = \sigma_0 Y_{II} \sqrt{\pi a} \tag{4}$$

where:

$$Y_I = Y_I' \left(1 - \frac{a}{W}\right)^{-3/2} \tag{5}$$

$$Y_{II} = Y_{II}' \left(1 - \frac{a}{W}\right)^{-1/2} \tag{6}$$

The values Y_I' and Y_{II}' are available for different ratios of a/W e L/W in [13]. The stress σ_0 can be calculated by replacing the maximum load obtained at the experiments in the following expression:

$$\sigma_0 = \frac{3 P_{max} S}{2 B W^2} \tag{7}$$

T-stress

According to Williams, [14], the linear-elastic tangential stress at the crack tip region can be expressed in polar co-ordinates r and θ as:

$$\sigma_{rr} = \frac{1}{\sqrt{2\pi r}} \cos\frac{\theta}{2} \left[K_I \left(1 + \sin^2\frac{\theta}{2}\right) \right] + T\cos^2\theta + O\left(\sqrt{r}\right) \tag{8}$$

$$\sigma_{\theta\theta} = \frac{1}{\sqrt{2\pi r}} \cos\frac{\theta}{2} \left[K_I \cos^2 \frac{\theta}{2} - \frac{3}{2} K_{II} \sin\theta \right] + T\sin^2\theta + O\left(\sqrt{r}\right) \tag{9}$$

$$\sigma_{r\theta} = \frac{1}{2\sqrt{2\pi r}} \cos\frac{\theta}{2} \left[K_I \sin\theta + K_{II} \left(3\cos\theta - 1\right) \right] - T\sin\theta\cos\theta + O\left(\sqrt{r}\right) \tag{10}$$

where higher order terms $O\left(\sqrt{r}\right)$ are ignored near the crack tip, since their contribution is negligible compared with the other terms. The crack tip parameters K_I, K_{II} and T depend on the geometry and loading configurations and can vary considerably for different specimens, [3], [11].

Equivalent stress intensity factor
In this study the equivalent stress intensity factor proposed by Irwin, [15], was considered:

$$K_{eq} = \sqrt{K_I^2 + K_{II}^2} \tag{11}$$

Organization of the paper
The 'Introduction' and the next section ('Inclined central crack') briefly present the concepts used throughout the work. The paper is organized into two main subjects: the experimental work performed, describing specimens, testing conditions and results, and the simulation of crack path for several mixed mode situations tested, using the finite element method and the Abaqus software.
The development of numerical tools allows to evaluate the influence of non-mode I loadings in the crack path and in the growth rate. The aim of this work is to analyse the propagation of pre-existing cracks under pure mode I, pure mode II and unstable mixed mode I-II loading conditions. Numerical simulations with two-dimensional models created in Abaqus software were performed, and validated by comparison with the analytical and experimental results. *T*-stress and stress intensity factors were obtained using the finite element method, together with the modified virtual crack closure technique (mVCCT) and/or the J-integral. Finally, the extended finite element method (XFEM) was used to predict the crack trajectory under different loading conditions.

INCLINED CENTRAL CRACK

As found in most textbooks, *e.g.* [16], the stress intensity factors in mode I and II, for the case of a inclined central crack subjected to a remote tension are, [2]:

$$K_I = \sigma_y^\infty \sqrt{\pi a} = \sigma\sin^2\beta\sqrt{\pi a} \tag{12}$$

$$K_{II} = \tau_{xy}^\infty \sqrt{\pi a} = \sigma\sin\beta\cos\beta\sqrt{\pi a} \tag{13}$$

Later, *T*-stress for that geometry was found to be, *e.g.* [3]:

$$T = \sigma\cos\left(2\beta\right)\sqrt{\pi a} \tag{14}$$

Fig. 3 compares these analytical solutions with numerical values obtained with mVCCT and J-integral techniques. In this Figure, the stress intensity factor values are made non-dimensional by $\sigma\sqrt{\pi a}$.
Fig. 3 recalls the variation of the stress intensity factors as function of the angle *β*. For *β*=90° the stress intensity factor in mode I is obtained, but for *β*=0° both modes I and II disappear; *T* is the only non-zero parameter, implying that, for low *β* values, the fracture is dominated by *T*. It is also verified that, as expected, normalized *T* (*T*/*σ*) varies between -1 and 1, that is, between $T = -\sigma_{remote}$ for *β*=90° and $T = \sigma_{remote}$ for *β*=0°.
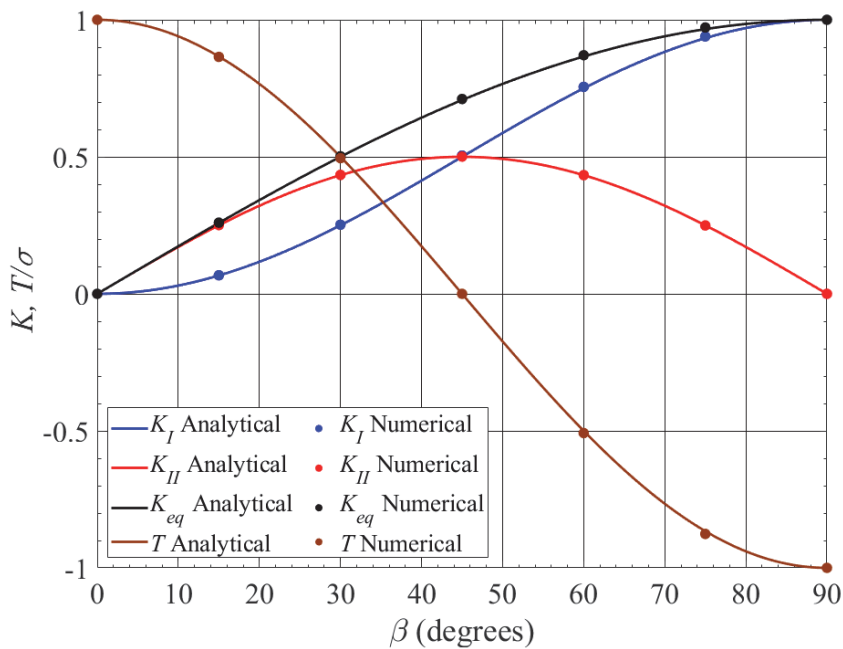
Figure 3: Numerical and analytical results.
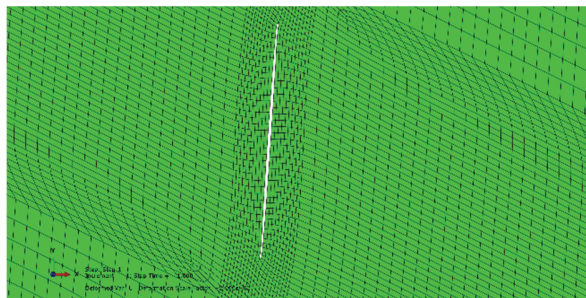
a) Propagation of the crack at 15°
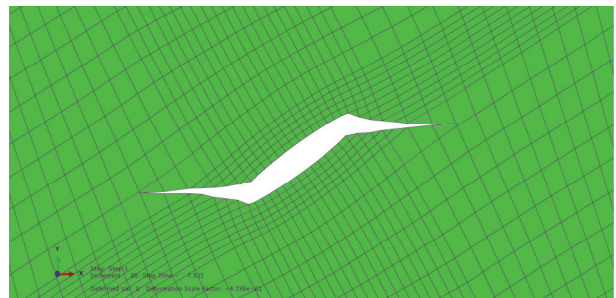

b) Propagation of the crack at 60°.
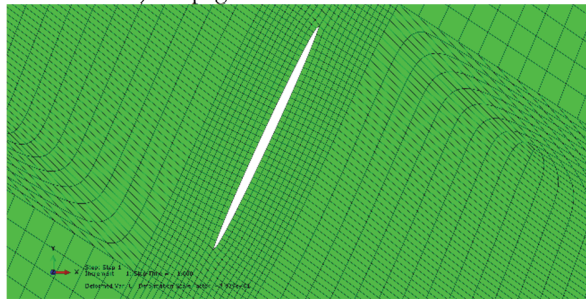
c) Propagation of the crack at 30°,
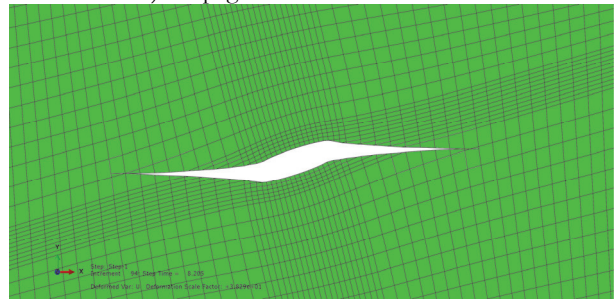
d) Propagation of the crack at 75°.
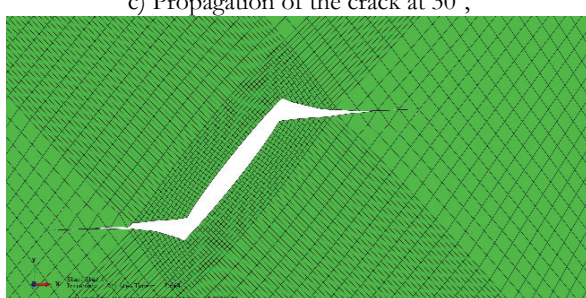
e) Propagation of the crack at 45°,
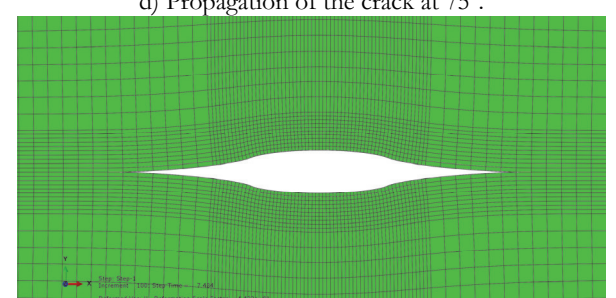
f) Propagation of the crack at 90°.

Figure 4: Propagation of the crack for different β values.

Fig. 4 shows how the crack propagates in each of the cases considered above, using the XFEM tool made available by Abaqus, that enables the study of the initiation and propagation of a crack in quasi-static problems.

Two different analytical methods presented in [17] are now compared with the analytical results obtained from Eqn. (14), for an angle of 60°. The following equations relate to the stress and deformation methods, Eqns. (15) and (16), respectively.

$$T = \frac{1}{2}[(\sigma_{xx})_{\theta=-\pi} + (\sigma_{xx})_{\theta=\pi}]$$ (15)

$$T = \frac{1}{2}E'\left[\left(\frac{dx_x}{dx}\right)_{\theta=-\pi} + \left(\frac{dx_x}{dx}\right)_{\theta=\pi}\right]$$ (16)

Fig. 5 shows a graphical comparison of the results achieved with these two methods. A similar approach is followed by [17].
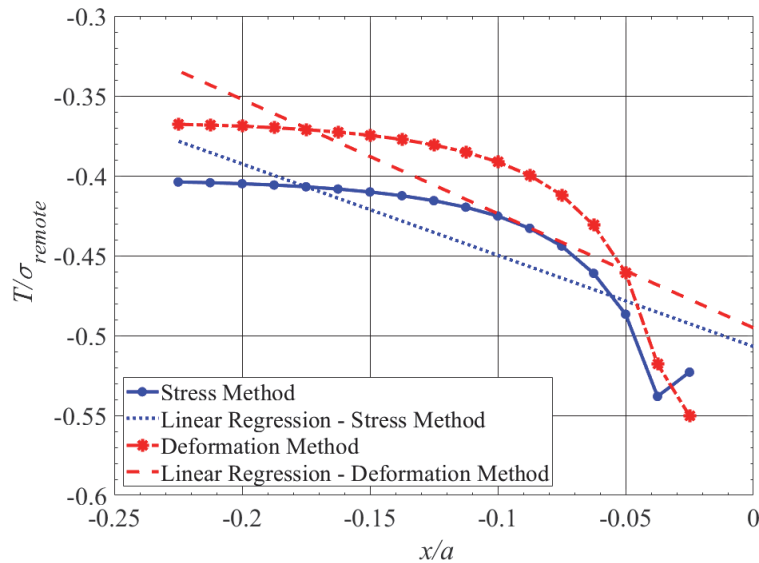

Figure 5: *T* for $\beta = 60°$.

The stress method provided a non-dimensional *T* value of -0.51, while the deformation method provided a value of -0.49, both agreeing with -0.5 obtained analytically. Because of the singularity the points closer to the crack tip were neglected in the regression lines. The consideration of the points very close to the crack tip would introduce larges errors in the evaluation of *T* values.

SPECIMENS

Four types of specimens in polymethyl methacrylate (PMMA) were considered. PMMA is a brittle material, transparent and colourless, which allows a direct observation of the crack tip. In this study cast PMMA was used, with Young´s modulus of 3.3 GPa, Poisson coefficient 0.3 and ultimate tensile strength 76 MPa. Fig. 7 a) shows the specimen used in the 4-point bending tests, and Fig. 7 b) the specimen used to achieve mixed mode in 3-point bending. Eleven 4-point bending tests were performed using an MTS servo-hydraulic machine under displacement control at 0.2 mm/min. The upper rollers had a diameter of 12.5 mm and the lower ones 30 mm. Since the lower part of the assembly had a predefined distance of 100 mm, the distance between supports was always maintained within the same 100 mm, varying only the supports position along the length of the specimen and its distance to the point of application of the load. For the 3-point bending, the same distance of 100 mm between rollers was maintained, as well as the displacement speed. The calibration of the non-standard 3-point bending specimen was performed using Abaqus software and J-integral.

Fig. 6 a) illustrates the negative consequences of an inadequate choice of points for extrapolating the T value. Calculation of T stress considering elements at unreasonable short distances from the end of the crack, including the extremity itself ($x/a=0$), culminates in values that are unrealistic. This is shown in Fig. 6, and is also discussed in [17].
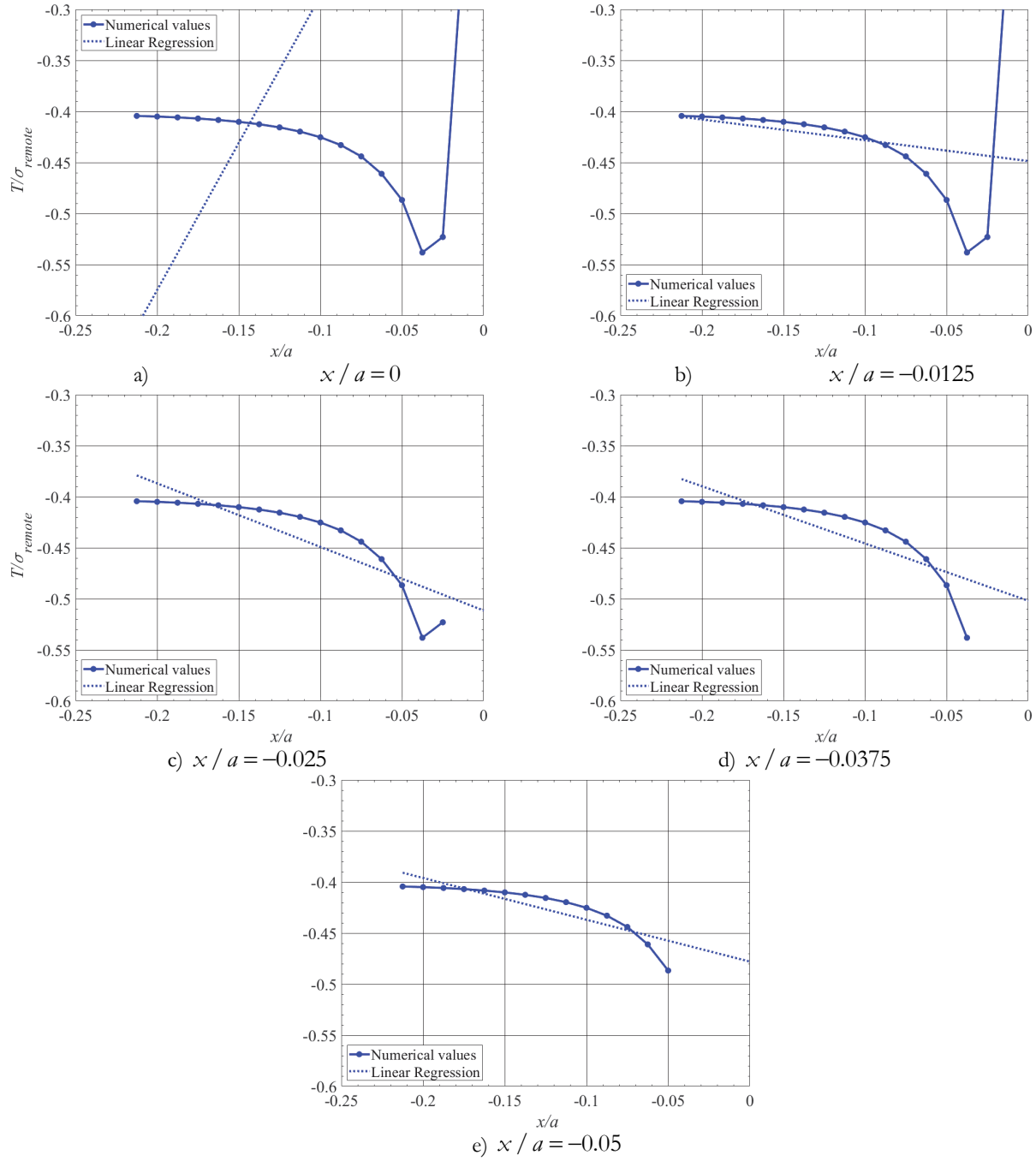

Figure 6: Variation of normalized T value for β=60°, Stress Method.

Fig. 8 a) presents the specimen to obtain the value of K_{Ic} according to the ASTM E399 standard. Fig. 8 b) presents a specimen with a slight difference from the previous one, for which an independent calibration using Abaqus software was performed.
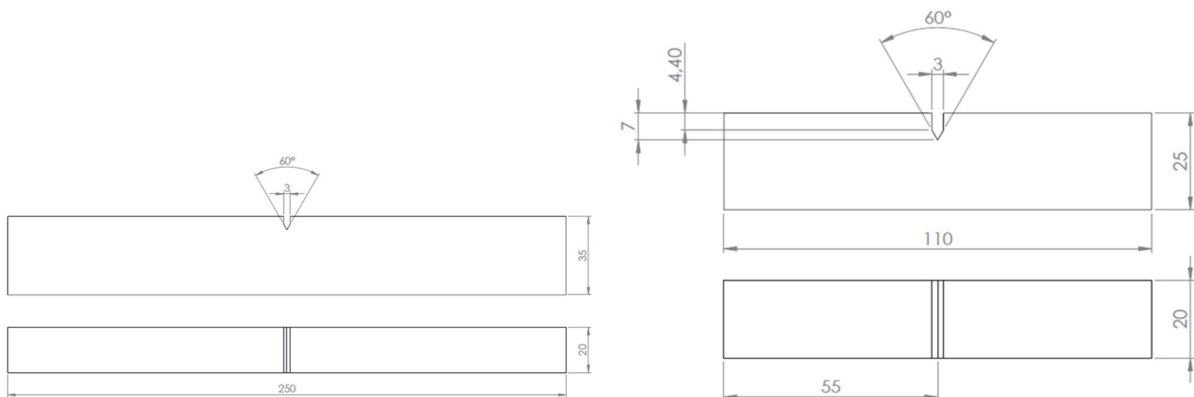
Figure 7: left, 4-point bending; right, 3-point-bending (mixed-mode).
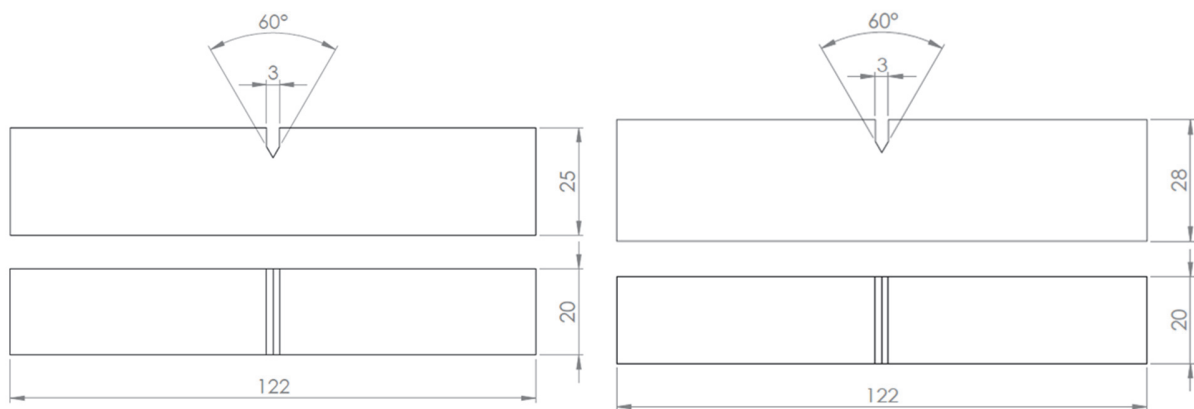
Figure 8: left, 3-point bending (ASTM E399); right, 3-point bending (non standard).

FOUR-POINT BENDING

Fig. 9 shows the experimental results obtained in laboratory for different ratios of K_I / K_{II}. These tests were also performed using an MTS servo-hydraulic machine, under the same displacement speed and control mode as mentioned above.

A simple representation of K_I/K_{II} *versus* φ_0, according to the Maximum Tangential Stress (MTS) criterion was obtained from Eqns. (17) and (18), presented in Fig. 10 a). In Fig. 10 b) the points obtained from the substitution of the maximum load recorded per specimen in Eqns. (1) and (2), are compared with the analytical curves.

$$\frac{K_I}{K_{II}} = \frac{1 - 3\cos\varphi}{\sin\varphi} \tag{17}$$

$$\frac{K_I}{K_{II}} = 1 \rightarrow \varphi = -0.92729[rad] = -53.13° \tag{18}$$

The experimental values can still be plotted against a theoretical curve that represents the kink angle as a function of the pre-crack angle and the mixity parameter M_e, once again according to the MTS criterion, Fig. 11. This curve is obtained from Eqns. (19) and (20). M_e is a trigonometrical function K_I and K_{II} presented by [3].

a) K_I/K_{II} =0 specimen 1

b) K_I/K_{II} =0.18 specimen 2

c) K_I/K_{II} =0.234 specimen 2b

d) K_I/K_{II} =0.540 specimen 3

e) K_I/K_{II} =0.899 specimen 6

f) K_I/K_{II} =0.932 specimen 4

g) K_I/K_{II} =1.799 specimen 7

h) K_I/K_{II} =1.857 specimen 5

i) K_I/K_{II} =2.232 specimen 7b

h) K_I/K_{II} =2.811 specimen 8

k) K_I/K_{II} =3.749 specimen 9
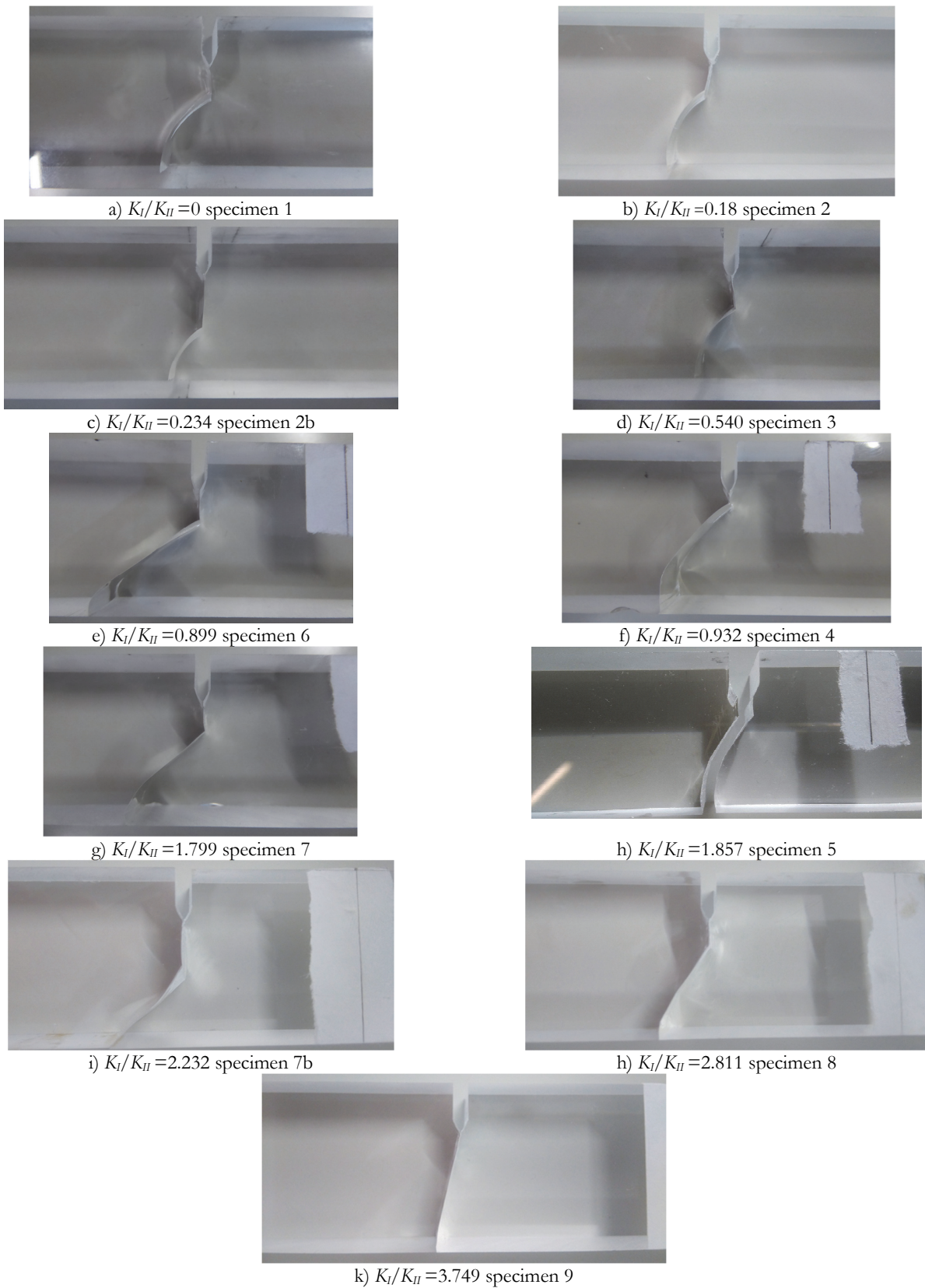
Figure 9: Crack propagation for different ratios of K_I / K_{II} .
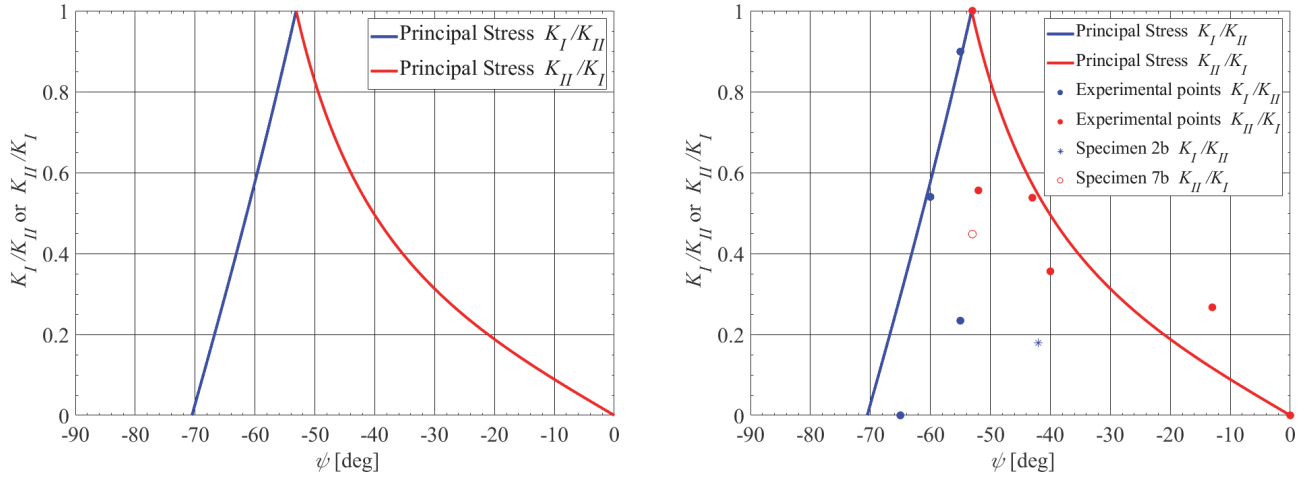
Figure 10: a) Relation between K_I/K_{II} and φ_0 for the MTS criterion, b) Experimental data.

$$\cot\beta = \frac{-\sin\varphi_0}{3\cos\varphi_0 - 1} \tag{19}$$

$$M_e = \frac{2}{\pi}\tan^{-1}\left(\frac{K_I}{K_{II}}\right) \tag{20}$$

$$M_e = \frac{2}{\pi}\tan^{-1}\left(\frac{\text{sen}\beta}{\cos\beta}\right) = \frac{2}{\pi}\tan^{-1}\left(\tan\beta\right) = \frac{2}{\pi}\beta \tag{21}$$
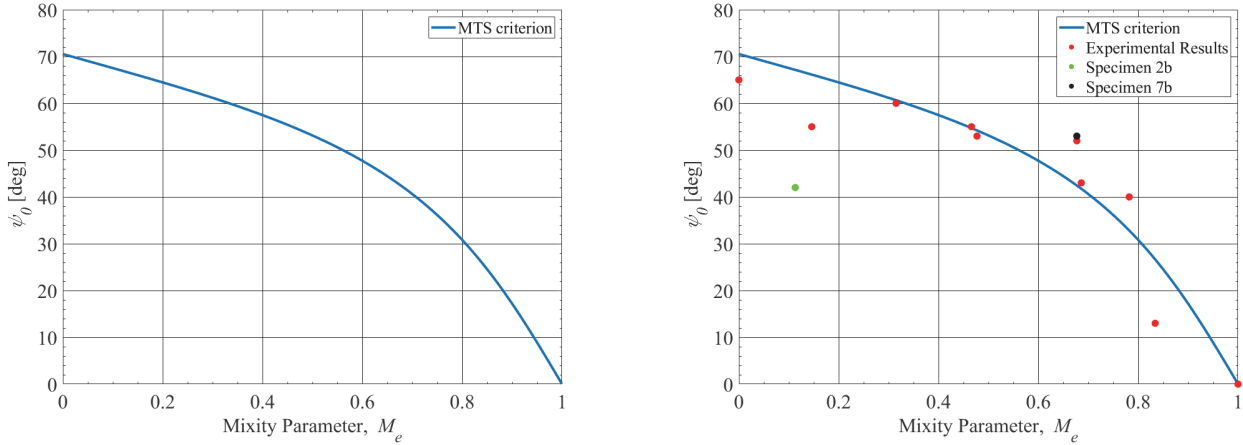

Figure 11: a) Kink angle function of the pre-crack angle and mixed mode, b) Experimental points.

The mixed mode criteria used to compare with experimental data are presented in the Eqns. (22) to (28), Fig. 12.

MTS

$$K_I\left(3\cos\frac{\varphi_0}{2} + \cos\frac{3\varphi_0}{2}\right) - 3K_{II}\left(\sin\frac{\varphi_0}{2} + \sin\frac{3\varphi_0}{2}\right) = 4K_{Ic} \tag{22}$$

$$\varphi_0 = -\arccos\left(\frac{3K_{II}^2 + K_I\sqrt{K_I^2 + 8K_{II}^2}}{K_I^2 + 9K_{II}^2}\right) \tag{23}$$

SED

$$\left(\frac{K_I}{K_{Ic}}\right)^2 = \frac{2(\kappa-1)m^2}{a_{11}m^2 + a_{12}m + a_{22}} \tag{24}$$

$$\left(\frac{K_{II}}{K_{Ic}}\right)^2 = \frac{2(\kappa-1)}{a_{11}m^2 + a_{12}m + a_{22}} \tag{25}$$

$$\begin{aligned}
a_{11} &= \left[(1+\cos\varphi)(\kappa-\cos\varphi)\right] \\
a_{12} &= 2\sin\varphi(2\cos\varphi-\kappa+1) \\
a_{22} &= \left[(\kappa+1)(1-\cos\varphi)+(1+\cos\varphi)(3\cos\varphi-1)\right]
\end{aligned} \tag{26}$$

$$\begin{cases}
\kappa = 3-4\nu \text{ , } \textit{for plane stress} \\
\kappa = \dfrac{3-\nu}{1+\nu} \text{ , } \textit{for plane deformation}
\end{cases} \tag{27}$$

Circle

$$K_I^2 + K_{II}^2 = K_{Ic}^2 \tag{28}$$

Ellipse

$$\left(\frac{K_I}{K_{Ic}}\right)^2 + \left(\frac{K_{II}}{K_{IIc}}\right)^2 = 1 \tag{29}$$
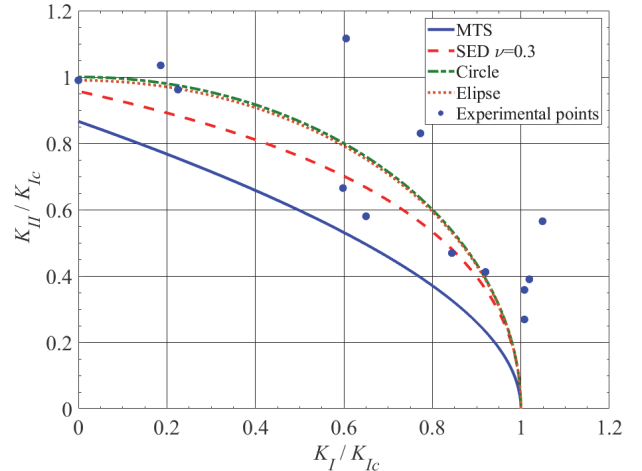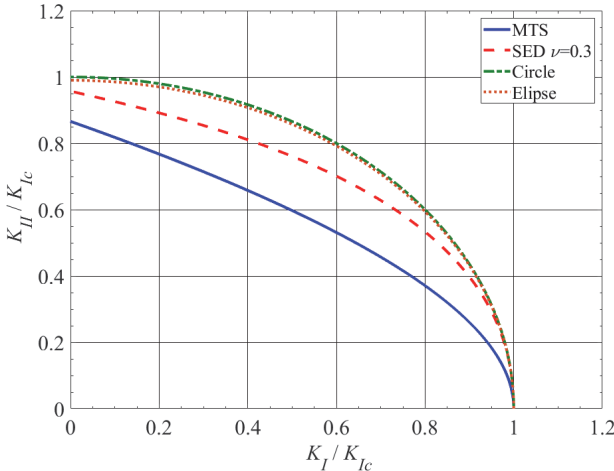

Figure 12: a) Mixed mode fracture according to the MTS criterion, SED, ellipse and circle, b) Experimental points.

In his presentation of the Strain Energy Density (SED) criterion, [18], Sih found that this was closer to the experimental points obtained in the earlier experiments of Erdogan and Sih, [2]. In the present work the same situation was verified, Fig. 12, although the circle seems to be an even better approximation of the presented experimental points.

THREE POINT BENDING RESULTS

For the 3-point bending tests, K_{Ic}=1.4 MPa$\sqrt{m}$ was obtained for the non-standard specimen (two tests), and K_{Ic}=1.5 MPa$\sqrt{m}$ for the specimens with standard geometry (two tests). The average K_{Ic}=1.45 MPa$\sqrt{m}$ was considered. The results obtained for the 3-point bending mixed mode experiments are presented in Tab. 1.

SPECIMEN	K_I $\left[\mathbf{MPa}\sqrt{\mathbf{m}}\right]$	$K_{II}\left[\mathbf{MPa}\sqrt{\mathbf{m}}\right]$	φ_0 [°]	$\varphi_{0\ expected}$ [°]
9	1.451	0.565	58	69
10	0.889	0.960	52	43

Table 1: Values of K_I and K_{II}, as the angles expected according to the MTS criterion, and the ones obtained.

T-STRESS RESULTS

Fig. 13 a) shows the values of *T*-stress obtained in Abaqus software for the specimens tested in 4-point bending. Fig. 13 b) shows the values obtained in three point bending tests for a range of a/W values.

In Fig. 13 a) the value of the *T* stress made non-dimensional using Eqn. (7) is presented as a function of the mixed mode parameter M_e. The correlation value between the experimental points and a linear regression is also presented. Fig. 13 b) shows the increase of *T* values with the increase of the a/W ratio. Eqn. (15) was used to evaluate the *T*-stress. The simulations were performed with linear quadratic elements (reference CPS4 in Abaqus) with 1 mm element length.
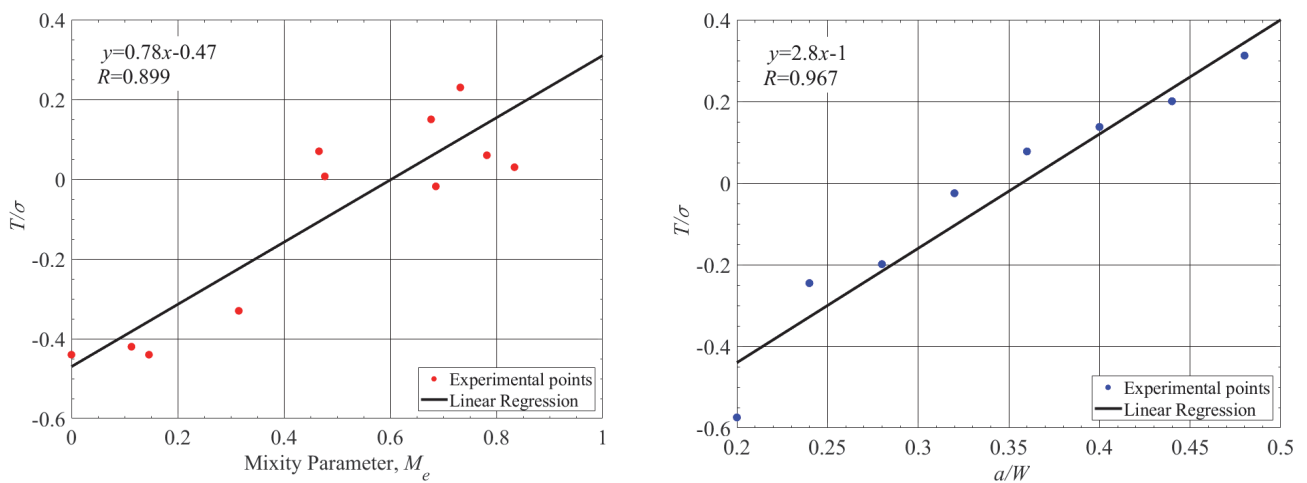

Figure 13: a) 4-point bending test specimens, b) 3-point bending simulation 0.2<a/W<0.5.

CRACK PROPAGATION: EXPERIMENTS AND SIMULATION

T he crack propagation was modelled using Abaqus and compared with the experimental results. The following figures show these comparisons for the case of 4-point bending with 2D and 3D simulations, and 2D simulations for the 3-point bending tests.
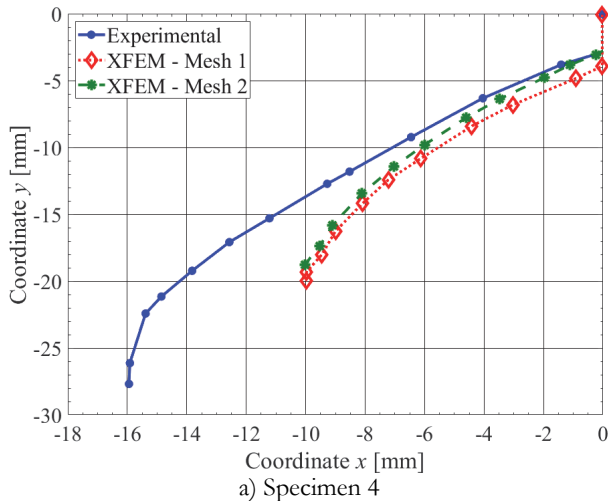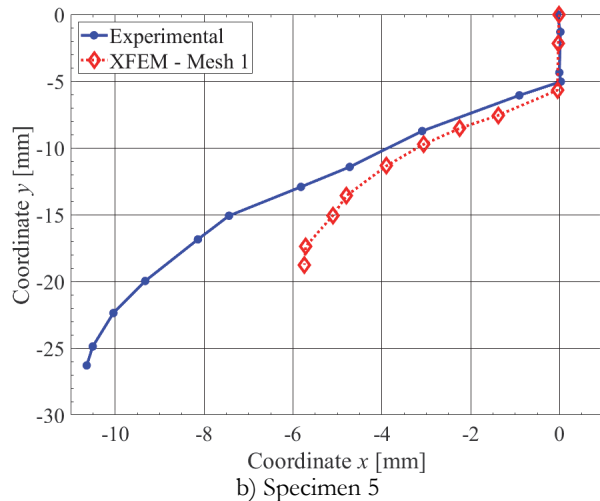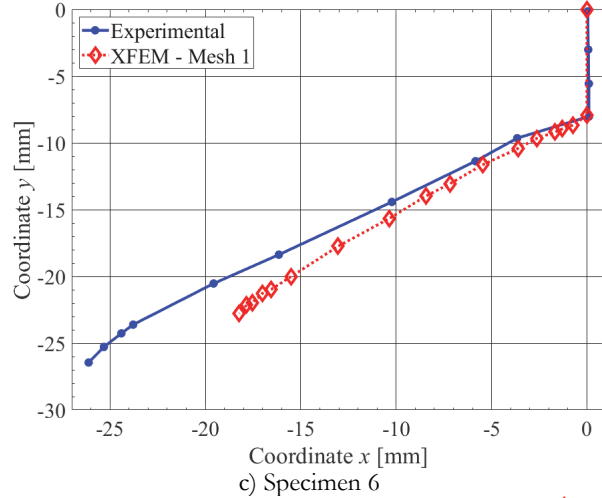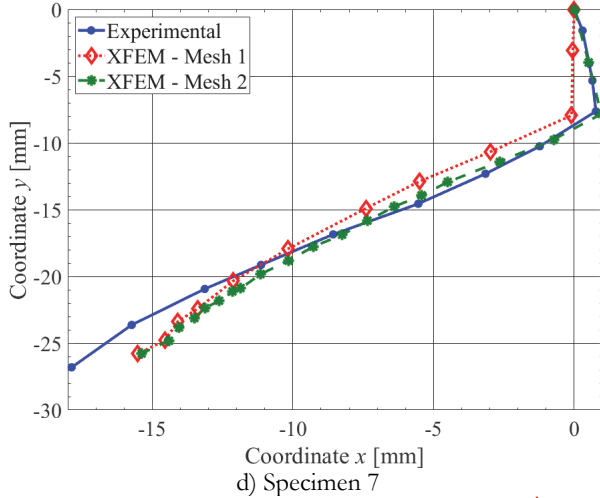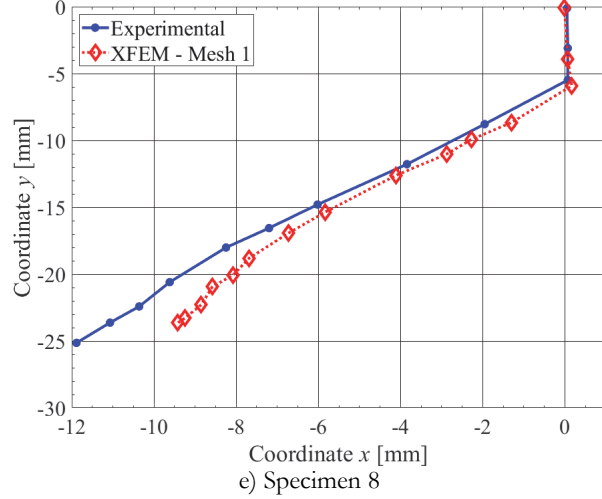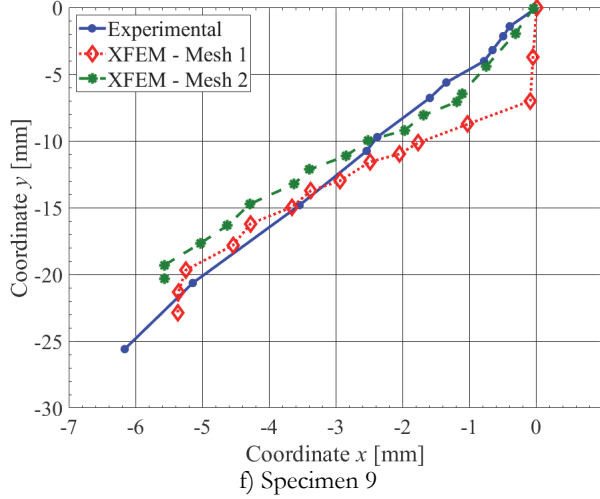

Figure 14: Comparison of the pre-crack resisted and the simulation for 2D 4-point bending.

Four-point bending - crack path with 2D elements
Fig. 14 shows a graphic comparison between the crack path obtain in laboratory and the one obtained with the software. The pre-crack of specimens 4, 7 and 9 had a slight initial inclination, since the process of making the pre-crack is manual, which implies that it is not totally controllable. So, two simulations were carried out, one in which the pre-crack was as obtained in the process of making the pre-crack (red curve), and another with the nominal geometry (green curve).

Three-point bending - crack path with 2D elements
At this point the comparison between the crack paths in the case of 3-point and mixed-mode bending is presented. In the case of pure mode I, the propagation is not presented since it takes place at 0 degrees, as expected.
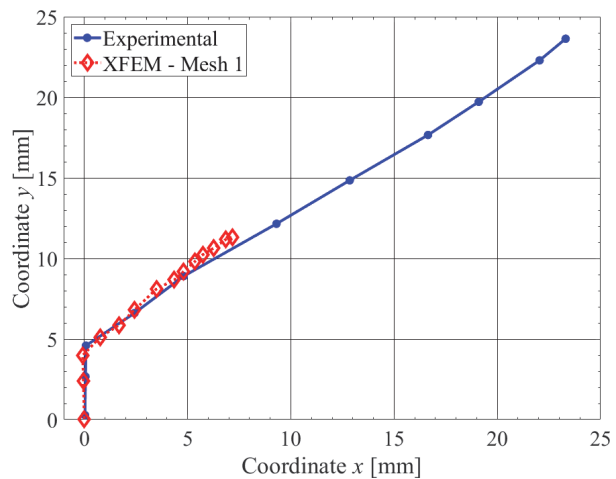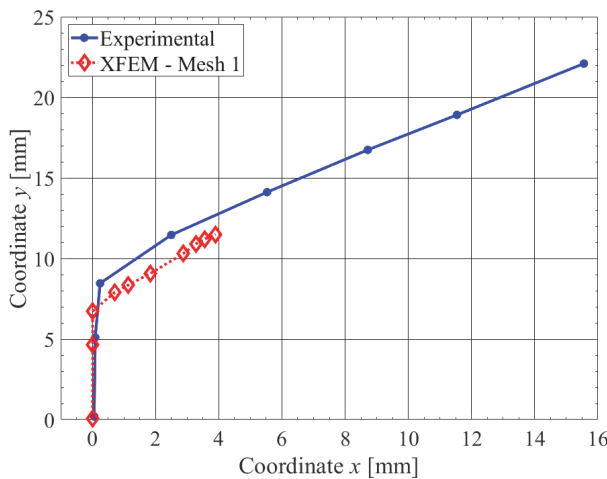

Figure 15: a) Specimen 3PB-9, b) Specimen 3PB-10.

For both test specimens there is a good agreement between the simulated and experimental paths, although it was not possible to obtain a longer propagation using XFEM models, Fig. 15.

Four-point bending - crack path with 3D elements
Fig. 16 shows a comparison between crack paths for specimen 4. Both the 2D and the 3D simulations show a good agreement with the experimental path, for the early stages of propagation, although the 3D seems to culminate in a more consistent prediction of the crack path.
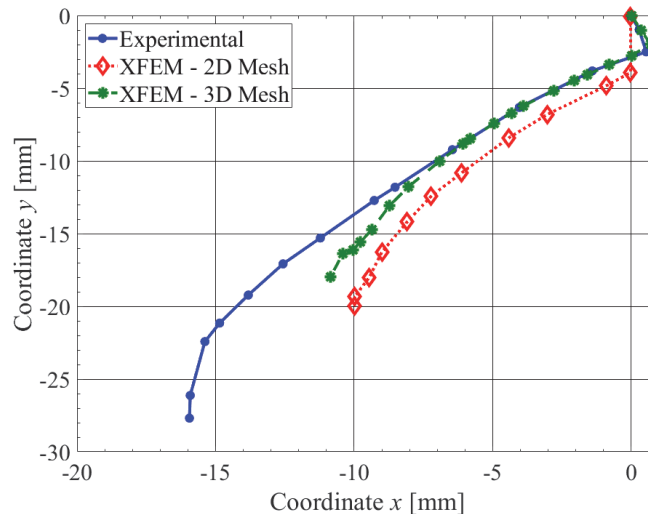

Figure 16: Specimen 4, 2D and 3D.

Fig. 17 presents the simulated propagation of the pre-crack in three-dimensional Abaqus software, and comparison with the experimental results. The specimens 5, 7 and 9 were simulated with two mesh configurations: unstructured – Mesh 1 and structured – Mesh 2, resulting in minor differences.
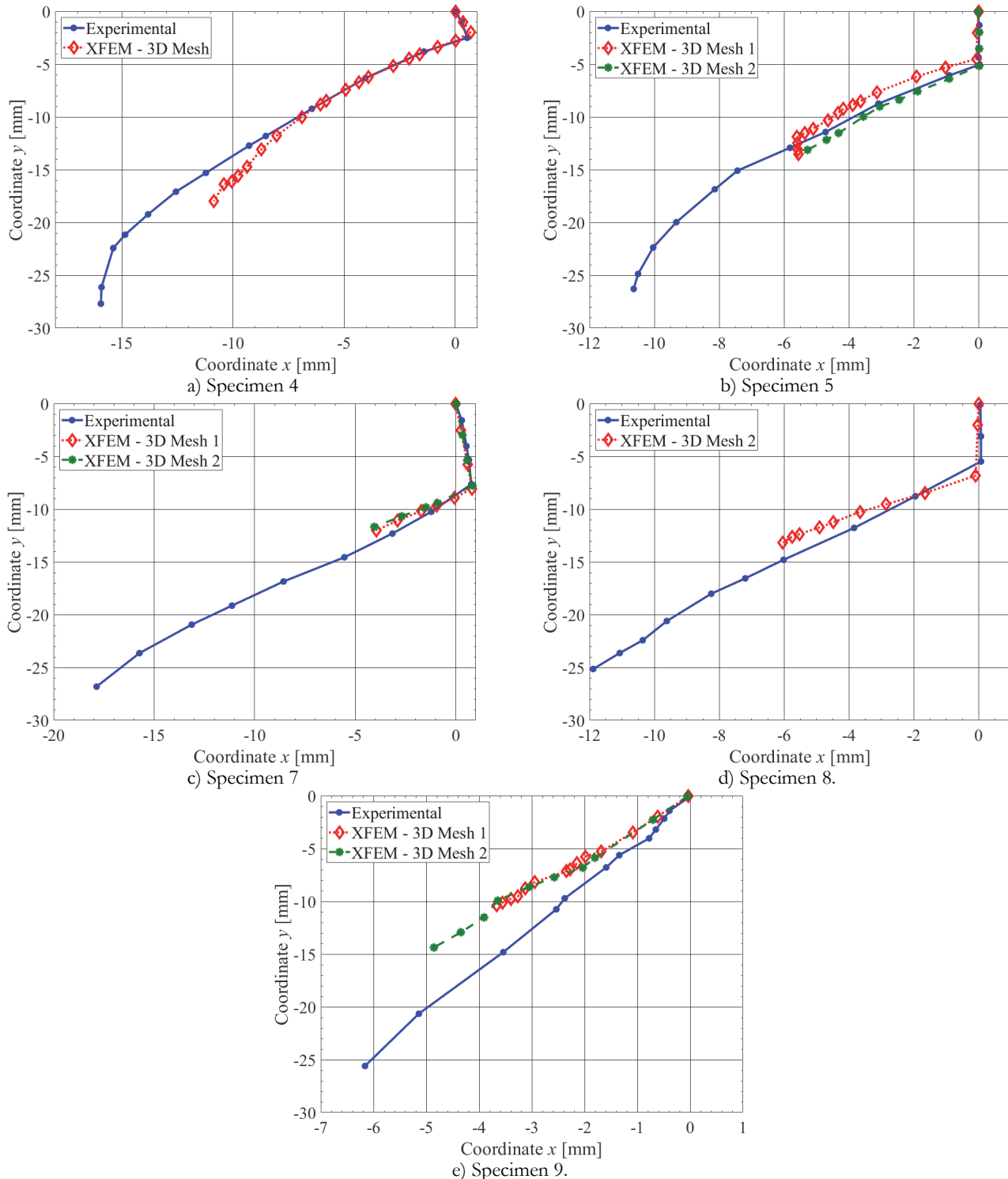

Figure 17: Comparison of the pre-crack resisted and the simulation for 3D 4-point bending.

CONCLUDING REMARKS

Fracture tests on 4- and 3-point bending specimens of PMMA were carried out for mixed mode fracture analysis and numerical assessment with the extended finite element method (XFEM). Unlike other works, in the present experimental results no correlation between T-stress and the toughness level was found: all fracture points are above the MTS theoretical values, a result similar to the early tests of Erdogan and Sih in their classical tests of flat plates of PMMA with inclined cracks. The strain energy density (SED) criterion provides an improved lower bound fit of the experimental data points. Nevertheless, most of the experimental points are above of this curve, requiring further studies to evaluate this effect.

Concerning the crack path prediction with XFEM implemented in Abaqus, generally good agreement with experiments was obtained, particularly in the initial steps of crack propagation. XFEM analysis were performed using the MTS criterion, and it is noted that the crack path simulation may be slightly affected by the fracture criteria considered.

The results found for the inclined central crack plate remotely loaded by a tensile stress, show good consistency between *T*-stress results obtained either by analytical methods or directly or indirectly through Abaqus software.

ACKNOWLEDGEMENTS

REFERENCES

[1] Alkan, U., Tutluoglu, L. (2016). Investigation of beam specimen geometries under four-point asymmetric bending for shear mode fracture toughness measurements of rocks, Pap. ARMA (American Rock Mech. Assoc. 16-183, (October).

[2] Erdogan, F., Sih, G.C. (1963). On the crack extension in plates under plane loading and transverse shear, J. Basic Eng., 85(4), pp. 519.

[3] Smith, D.J., Ayatollahi, M.R., Pavier, M.J. (2000). The role of T-stress in brittle fracture for linear elastic materials under mixed mode loading, Fatigue Fract. Eng. Mater. Struct., 24(2), pp. 137–150.

[4] Richard, H.A. (1981). A new compact shear specimen, Int. J. Fract. 17(5), pp. 105–107.

[5] Atkinson, C., Smelser, R. E., Sanchez, J. (1982). Combined mode fracture via the cracked Brazilian disk test, Int. J. Fract. 18(4), pp. 279–291.

[6] Krueger, R. (2004). Virtual crack closure technique: history, approach, and applications, Appl. Mech. Rev. 57(2), pp. 109–143.

[7] Belytschko, T., & Black, T. (1999). Elastic crack growth in finite elements with minimal remeshing, Int. J. Numer. Methods Eng. 45(5), pp. 601–20.

[8] Rebelo, C.A.C.C. (1987).Caracterização do Comportamento à Fractura de Resinas Poliester Insaturadas, tese de Mestrado em Materiais e Processos de Fabrico. FEUP, 1987.

[9] He, M.Y., Hutchinson, J.W. (2000). Asymmetric four-point crack specimen, J. Appl. Mech., 67(March 2000), pp. 207–209.

[10] Ayatollahi, M.R., Aliha, M.R.M. (2011). On the use of an anti-symmetric four-point bend specimen for mode II fracture experiments, Fatigue Fract. Eng. Mater. Struct., 34(11), pp. 898–907.

[11] Wang, C., Zhu, Z.M., Liu, H.J. (2016). On the I–II mixed mode fracture of granite using four-point bend specimen, Fatigue Fract. Eng. Mater. Struct., 39(10), pp. 1193–1203.

[12] Belli, R., Wendler, M., Petschelt, A., Lohbauer, U. (2017). Mixed-mode fracture toughness of texturized LS2 glass-ceramics using the three-point bending with eccentric notch test, Dent. Mater., 33(12), pp. 1473–1477.

[13] Fett, T. (1991). Mixed-mode stress intensity factors for the thee-point bending bars, Int. J. Fract., 48, pp. 67–74.

[14] Williams, M.L. (1957). On the stress distribution at the base of a stationary crack, J. Appl. Mech., 24, pp. 109–114.

[15] Irwin, G.R. (1957). Analysis of stresses and strains near the end of a crack traversing a plate, J. Appl. Mech., 24, pp. 361–364.

[16] Arteiro, A.J.C., de Castro, P.M.S.T. (2014). Mecânica da Fratura e Fadiga: Exemplos de cálculo e aplicação, FEUP

Edições.

[17] Ayatollahi, M.R., Pavier, M.J., Smith, D.J. (1998). Determination of T-stress from finite element analysis for mode I and mixed mode I / II loading, Int. J. Fract., 91, pp. 283–298.

[18] Sih, G.C. (1991). Mechanics of fracture initiation and propagation, Springer.

SYMBOLOGY

a – crack length
B – specimen thickness
β – crack angle
E – Young's modulus
φ_0 – crack propagation angle
K – stress intensity factor
K_{eq} – equivalent stress intensity factor
K_I – stress intensity factor for mode I
K_{Ic} – critical stress intensity factor for mode I
K_{II} – stress intensity factor for mode II
K_{IIc} – critical stress intensity factor for mode II
K_{III} – stress intensity factor for mode III

κ - parameter for plane stress or strain
M_e – mixity parameter
P – applied load
Q – shear force on the crack tip
S – distance between rollers
S_0 – distance from the line of load application to the plane of the crack
σ – tensile stress; remote stress
T – T-stress
W – specimen width